Analytical models of the magnetic field of disk-shaped current sheets

N. A. Tsyganenko

Laboratory for Extraterrestrial Physics, NASA Goddard Space Flight Center, Greenbelt, Maryland

M. Peredo

Laboratory for Extraterrestrial Physics, Hughes STX Corporation at NASA Goddard Space Flight Center, Greenbelt, Maryland

Abstract. Disk-shaped current distributions are useful tools in modeling the magnetospheres of Earth and other planets and have also been adapted for modeling the geotail. Such models usually start with an axisymmetric vector potential but may be modified to account for observed asymmetries, variable thickness, and warping in response to an inclined orientation of the planetary dipole axis. Models of this type until now either have lacked the ability to simulate a sharp inner edge of the current and to control accurately its falloff with distance or did not allow a simple analytical representation. Here existing methods will be reviewed, after which a new class of models which overcomes the above deficiencies and also allows the modeling of current disks of finite thickness flanked by current-free regions will be presented.

1. Introduction

The empirical modeling of the magnetic field in planetary magnetospheres is best handled by a modular approach, that is, by developing separate representations for the principal components of the field and then adding them together. A commonly observed element of magnetospheric current systems is a warped current sheet of finite thickness that varies in space and time. In some cases, for example, in the magnetospheres of Jupiter and Saturn, the sheetlike currents are almost axisymmetrical; in the Earth's magnetosphere, however, certain asymmetries are observed in the ring current, and in addition the inner tail current sheet resembles a disk current confined within a relatively narrow sector of longitudes.

The most straightforward way of computing the magnetic field produced by any given current system is to calculate the Biot-Savart integral. However, spacecraft experiments provide the magnetic field data rather than the electric currents. Furthermore, not only is Biot-Savart integration too cumbersome a procedure for routine tracing of field lines, but it also fails to characterize the field by a small number of well-defined parameters which can be fitted to observations. Such fitting is essential for extracting from data the underlying distribution of electric currents [e.g., *Tsyganenko*, 1990] and thus justifying the precise configuration of **j** used by the model. To obtain the information from data, models should be based on flexible and simple analytical functions, which could yield a large variety of magnetic field configurations parameterized by weight coefficients and geometrical factors and satisfying some basic requirements, including the divergence-free condition $\nabla \cdot \mathbf{B} = 0$.

In this work we briefly survey existing methods for modeling various current sheets and then describe in more

detail a new analytical representation capable of reproducing a wide class of magnetic fields induced by an equatorial current sheet of finite thickness. As shown below, the method allows a further generalization, making it possible to model warped current sheets with a spatial variation of the current sheet thickness.

2. Models Based on the Spread-Out Current Filament Integration

Tsyganenko and Usmanov [1982] and *Tsyganenko* [1987] (referred to henceforth as TU82 and T87, respectively) proposed a simple and flexible model of the Earth's magnetospheric tail current sheet with a finite thickness constructed as a continuous distribution of infinitely long straight current filaments. Each filament is parallel to the y axis, carries a current dI, and lies in the equatorial plane $z = 0$, producing an axially symmetric magnetic field

$$d\mathbf{B} = \frac{\mu_0 \, dI}{2\pi} \frac{\rho}{\rho^2 + D^2} \mathbf{e}_\phi, \tag{1}$$

with circular force lines centered on the filament axis. At large distances from the axis ($\rho \gg D$), the ρ-dependent part of (1) tends to $1/\rho$, fitting a curl-free field from a thin wire, while for $\rho \leq D$ it varies as ρ/D^2, giving the field of a current density uniformly distributed in a cylinder. Approximating the tailward variation of the current density dI/dx by simple analytical functions (linear in TU82 and inverse powers of ($x - x_c$) in T87), the integration can be done analytically, resulting in compact expressions for B_x and B_z (see the original works for details). The B_y component remains identically zero, and this imposes some limitations on the model: it certainly works better in the far and middle tail regions, where the field is stretched along the Sun-Earth line, but worsens at dawn and dusk in the near tail, where the current flow lines approximate circular arcs. This deficiency was partially remedied in TU82 and T87 by introducing into

the expressions for B_x and B_z a "form factor" $f(y)$ which falls off toward the tail flanks and forces the current flow lines to bend in a desirable way, as shown in Figure 3 of TU82. However, such a "quick fix" solution is incapable of taking into account the observed geometry of the inner tail current sheet and the relatively large values of B_y on the dawn and dusk sides.

A search for a better representation of the near-tail magnetic field resulted in analytical models based on disklike equatorial current sheets [*Connerney et al.*, 1981; *Tsyganenko*, 1989a] (referred to henceforth as CAN81 and T89, respectively) that are briefly discussed in the next section.

3. Models Based on the Equatorial Current Disks

Another approach starts from the equation for the vector potential **A**. Assuming that all currents are confined to the equatorial plane $z = 0$, **A** everywhere else satisfies

$$\nabla \times \nabla \times \mathbf{A} = 0. \tag{2a}$$

We use cylindrical coordinates (ρ, ϕ, z) and assume axially symmetric azimuthal electric currents, which implies $A_\rho = A_z = 0$ and reduces (2a) to the following equation for the azimuthal component $A_\phi \equiv A$ of the vector potential:

$$\frac{\partial^2 A}{\partial z^2} + \frac{\partial}{\partial \rho}\left[\frac{1}{\rho}\frac{\partial(\rho A)}{\partial \rho}\right] = 0 \tag{2b}$$

Separation of variables leads to a general solution

$$A = \int_0^\infty C(\lambda)J_1(\lambda\rho) \exp(-\lambda|z|) \, d\lambda \tag{3}$$

where J_1 is the Bessel function. The function $C(\lambda)$ contains all relevant information on the distribution of the azimuthal electric current in the current sheet and can be completely defined by imposing appropriate boundary conditions.

One way to impose the boundary conditions, used in CAN81, is to specify the distribution of the electric current in the equatorial plane as

$$I(\rho) = \frac{2}{\mu_0}\left.\frac{\partial A}{\partial z}\right|_{z=0}, \tag{4}$$

where $I(\rho)$ is a given function of the radial distance from the axis of symmetry. This approach was successfully employed for constructing the CAN81 model of the Jovian current disk, in which the function $I(\rho)$ had an abrupt inner cutoff and fell off outward as ρ^{-1}; however, the assumed current profile did not allow all components of the magnetic field to be derived in a closed analytical form.

An alternative approach, developed in T89, is to specify the distribution of the transverse component of the magnetic field:

$$B_z(\rho) = \frac{1}{\rho}\left.\frac{\partial(\rho A)}{\partial \rho}\right|_{z=0}, \tag{5}$$

There is a very limited number of analytical approximations for $I(\rho)$ or $B_z(\rho)$ which, used as boundary conditions, yield the vector potential (3) in a compact analytical form. Among such functions for $B_z(\rho)$ is the form specified in T89:

$$B_z(\rho) \sim (a^2 + \rho^2)^{-1/2}, \tag{6}$$

providing maximal depression amplitude at the origin and a gradual outward decay of the disturbance field. Combining (6) with (5) and (3) and applying the Fourier-Bessel transform leads to a very simple analytical vector potential:

$$A(\rho, z) = C\rho^{-1}\{[(a + |z|)^2 + \rho^2]^{1/2} - (a + |z|)\}, \tag{7}$$

where a is the characteristic scale length, roughly corresponding to the position of the maximum of the electric current density. Substituting (7) in (2b), it can be easily verified that the vector potential is curl-free everywhere except on the equatorial plane. As shown in T89, one can obtain a family of independent current disk vector potentials by taking a sequence of derivatives of the "basic-mode" potential (7) with respect to the parameter a. We refer the reader to the original T89 and CAN81 papers for further details and proceed in the next section to describe a new family of solutions for the vector potential.

4. Axisymmetric Curl-Free Vector Potentials: A New Family of Basic-Mode Current Disk Models

The analytical vector potentials derived in T89 were used for modeling the magnetic field produced by the ring current and the tail current sheet in the Earth's magnetosphere. Special measures were taken to simulate the observed day-night asymmetry of the ring and tail current systems: the vector potentials were multiplied by appropriate truncation factors, the current sheet thickness was assumed to vary in the Sun-Earth direction, and warping of the current sheet due to the geodipole tilt was introduced through a modification of the z dependence. An advantage of using vector potentials is that none of these modifications violate the condition $\nabla \cdot \mathbf{B} = 0$.

However, the T89 model had two troublesome deficiencies. First, it failed to properly reproduce a steep profile of the electric current density in the vicinity of the inner edge of the current sheet, a feature that is at times indirectly evidenced at tailward distances of 5–8R_E [*Sergeev and Malkov*, 1988]. It also lacked the diamagnetic eastward ring current that exists in the inner L shells [e.g., *Lui et al.*, 1987]. Instead, the T89 equatorial current profile exhibited an approximately linear increase of the westward current $I(\rho)$ in the interval $0 < \rho \leq a$. Second, even for the "slowest-mode" vector potential (7), the current density decreased outward as ρ^{-2} for $\rho \gg a$, while the average observed decrease is much slower [e.g., *Behannon*, 1968]; this deficiency caused some problems with regard to correctly reproducing both B_x and B_z distributions in the tail [e.g., *Stern and Tsyganenko*, 1992; *Peredo et al.*, 1993].

These considerations motivated us to develop further the analytical modeling of the tail current system. Our general approach was to find analytical solutions to (2b) yielding the desired current distribution near the axis of symmetry and having different variation scales at larger distances. Once such a family of basic functions is obtained, one can easily match a wide variety of electric current profiles by constructing appropriate linear combinations of the analytical solutions.

The starting point of the present study is to specify a
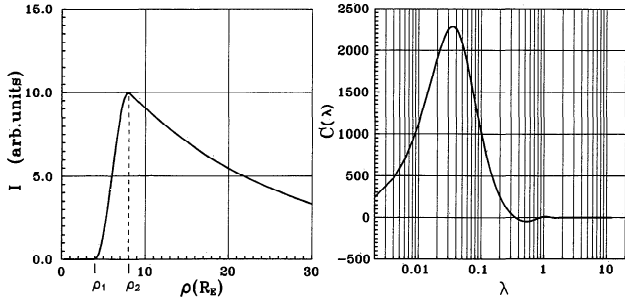
Figure 1. (Left) Variation of the electric current density in the equatorial current disk with radial distance as prescribed by the original model (8); (right) plot of the corresponding Fourier-Bessel amplitude $C(\lambda)$.

desirable profile for the electric current. We have chosen it as a piecewise-continuous function

$$
\begin{aligned}
I(\rho) &= 0 & \rho &< \rho_1 \\
I(\rho) &= I_m \sin^2\left(\frac{\pi}{2}\frac{\rho - \rho_1}{\rho_2 - \rho_1}\right) & \rho_1 &< \rho < \rho_2 \\
I(\rho) &= I_m \exp\left(\frac{\rho_2 - \rho}{L}\right) & \rho &> \rho_2
\end{aligned}
\tag{8}
$$

displayed in Figure 1 (left panel) and completely defined by its peak value I_m, the parameters of the inner slope ρ_1 and ρ_2, and the e-folding scale L of the descending outer part of the profile. The plot in the right panel of Figure 1 shows the typical shape of the Fourier-Bessel amplitude $C(\lambda)$ corresponding to the function (8) and found by numerically evaluating the integral

$$
C(\lambda) = \frac{\mu_0}{2} \int_0^\infty J_1(\lambda\rho)I(\rho)\ \rho\ d\rho
\tag{9}
$$

As seen in the plot, the function $C(\lambda)$ is characterized by a rapidly decaying oscillatory behavior, suggesting an expansion of the form

$$
C(\lambda) \approx \sum_{i=1}^{N} f_i \exp\left(-\alpha_i\lambda\right) \sin\left(\beta_i\lambda\right).
\tag{10}
$$

as a possible candidate for fitting the function $C(\lambda)$ by least squares. An outstanding advantage of the expansion (10) is that it allows the integral (3) to be expressed in a closed analytical form. Moreover, it was found in initial test runs that the least squares fits of the curve for $C(\lambda)$ in Figure 1 by the sum (10), even with $N = 2$, yielded the accuracy within a few percent. Thus encouraged, we chose to base our model on the representation (10); however, instead of fitting $C(\lambda)$ as given by (10), we fitted to (8) the corresponding analytical function for the electric current that follows from (10) upon substitution in (3) and subsequent derivation of $I(\rho)$ from (4). To reduce the number of free parameters, we assumed $\alpha_i = \beta_i$ in (10) and, after inserting it in (3), obtained

$$
A = \sum_{i=1}^{N} f_i \int_0^\infty J_1(\lambda\rho) \exp\left[-\lambda(\beta_i + |z|)\right]
$$

$$
\cdot \sin\left(\beta_i\lambda\right)\ d\lambda = \rho \sum_{i=1}^{N} f_i \frac{t_i(1 - t_i^2)^{1/2}}{S_{1i}S_{2i}},
\tag{11}
$$

where

$$
S_{1i} = [(\beta_i + |z|)^2 + (\rho + \beta_i)^2]^{1/2},
$$

$$
S_{2i} = [(\beta_i + |z|)^2 + (\rho - \beta_i)^2]^{1/2},
$$

$$
t_i = \frac{2\beta_i}{S_{1i} + S_{2i}}
$$

Equation (11) can be verified by using formula 6.752.1 of *Gradshteyn and Ryzhik* [1980], which after taking the derivative with respect to the parameter b, yields the result in the right-hand side of (11). The corresponding distribution of the electric current density in the equatorial plane follows from (4):

$$
\begin{aligned}
I(\rho) &= -\frac{2}{\mu_0}\frac{\partial A}{\partial z}\bigg|_{z=0} \\[2mm]
&= -\frac{2\rho}{\mu_0}\sum_{i=1}^{N}\frac{f_i}{S_{1i}S_{2i}} \\[2mm]
&\cdot\left\{\frac{\partial t_i}{\partial z}\left[(1 - t_i^2)^{1/2} - \frac{t_i^2}{(1 - t_i^2)^{1/2}}\right]\right. \\[2mm]
&\left. - t_i(1 - t_i^2)^{1/2}\frac{\partial \ln (S_{1i}S_{2i})}{\partial z}\right\},
\end{aligned}
\tag{12}
$$

and this is the analytical function used for fitting the current profiles (8).

5. Application to the Ring Current and Magnetospheric Tail

The next step was to choose several basic-mode functions (8) with different rates of tailward decrease of the electric current density and to find best-fit values for N coefficients f_i and N nonlinear parameters β_i. The calculations reported here were done for $N = 7$, $\rho_1 = 4$, $\rho_2 = 8$, and five values of the e-folding distance: $L = 100, 40, 15, 8,$ and 4 (all the distances are given in arbitrary units, e.g., in planetary radii). The first value yields the slowest variation of $I(\rho)$ and thus the most extended current disk, while the last one represents a sharply peaked current confined within the interval $5 \leq \rho \leq 15$. We also experimented with more localized profiles which rise and fall like a sinusoidal wave given in the middle part of (8) extended over the entire interval $\rho_1 < \rho < 2\rho_2 - \rho_1$.

Sample results of the least squares fitting are shown in Figures 2 and 3. Figure 2 displays long-range plots of the electric current profiles for the entire fitting interval $0 < \rho < 300$. The curves correspond to three values of L; in each plot the original functions (8) and the corresponding approximations (12) are graphed as solid and broken curves, respectively (the difference is almost indistinguishable in the plots for $L = 15$ and 40). Four panels in Figure 3 show the current density profiles on a magnified scale along the ρ axis in order
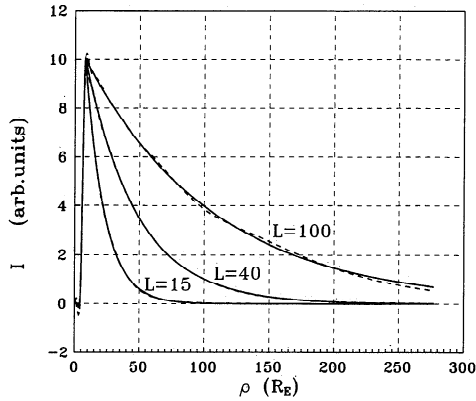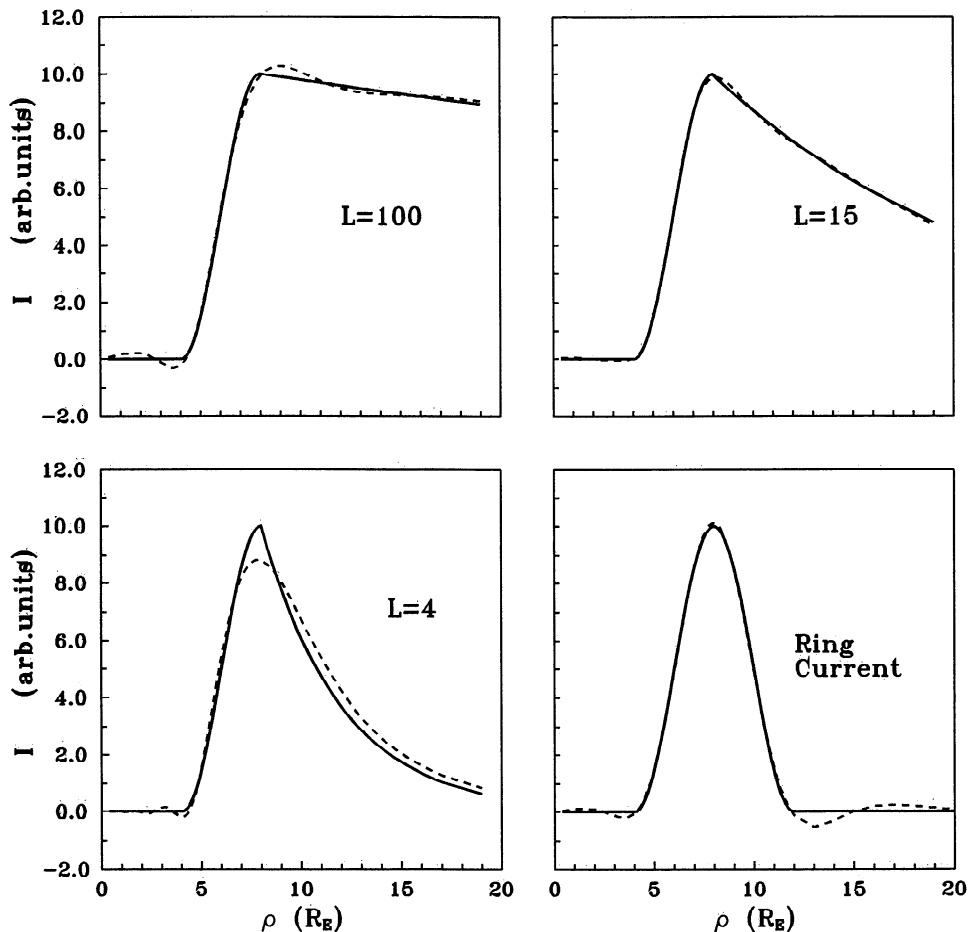
Figure 2. Plots of the electric current density for three values of the e-folding distance L. The solid curves correspond to the original distribution (8), and the broken curves are those given by best-fit seven-term expansions (12).

to better illustrate details in the inner region. In all cases, the seven-term expansions (12) accurately reproduce the current profiles. The values of the coefficients f_1 to f_7 and the parameters β_1 to β_7 for the six models are listed in Table 1. By combining the six solutions into a linear superposition of six vector potentials (11) with appropriate weight factors,

one can match a wide class of possible axisymmetric magnetic field distributions produced by infinitely thin equatorial current disks with various radial profiles of the electric current density, ranging from a very extended one given by the slowest-mode solution with $L = 100$ to a very localized ring current (Figure 3, top left and bottom right panels, respectively). Of course, the number of basic mode functions (six) as well as the number of terms $N = 7$ in the expansions (11) and (12) may be varied according to the required accuracy and the scatter in the input magnetic field data. The purpose of the present work is simply to describe the method rather than recommend a specific format.

As indicated above, all six sets of coefficients given in Table 1 correspond to the same position and slope of the inner edge of the current profile defined by the particular choice of the parameters $\rho_1 = 4$ and $\rho_2 = 8$. However, the models obviously allow an additional degree of freedom through an appropriate scaling of the radial distance ρ. Namely, it is easy to verify from (9) and (3) that any scaling transformation of a given electric current profile $I'(\rho) = I(\kappa\rho)$ leads to a modified vector potential $A'(\rho, z) = \kappa^{-1} A(\kappa\rho, \kappa z)$ and hence $\mathbf{B}'(\rho, z) = \mathbf{B}(\kappa\rho, \kappa z)$. In other words, the radial scaling of the current generates a family of self-similar magnetic fields.

The next step in generalizing the model is to modify the vector potential (11) by replacing $|z|$ by a smooth function in

Figure 3. Plots of the electric current density similar to those in Figure 2 but on a magnified horizontal scale, showing detailed shapes of the profiles near the origin.

Table 1. Coefficients f_i and Nonlinear Parameters β_i for the Current Disk Models With Different Rates of Outward Decrease of Current Density

| | Value at e-Folding Length Given | | | | | |
	$L = 100$	$L = 40$	$L = 15$	$L = 8$	$L = 4$	Ring Current
f_1	0.891397E+05*	0.110383E+05	0.283794E+04	0.118616E+04	0.162956E+04	0.325977E+09
f_2	0.309039E+05	0.835763E+04	0.223097E+04	0.252925E+04	−0.999837E+03	−0.381152E+09
f_3	0.830897E+04	0.484295E+04	−0.110543E+05	−0.233342E+04	0.604064E+03	−0.994041E+08
f_4	0.288275E+04	0.735456E+04	0.218400E+05	0.818938E+03	−0.294699E+03	0.161100E+09
f_5	0.376743E+04	−0.128267E+07	−0.200364E+05	−0.175597E+03	0.338718E+02	−0.652105E+07
f_6	−0.325129E+04	0.226321E+07	0.898058E+04	0.345697E+02	−0.532189E+01	−0.287028E+03
f_7	0.992913E+02	−0.986108E+06	−0.829337E+01	−0.427391E+01	0.398828E+00	0.388412E+02
β_1	0.111671E+03	0.599926E+02	0.204500E+02	0.127500E+02	0.545000E+01	0.816698E+01
β_2	0.508541E+02	0.355469E+02	0.941250E+01	0.500500E+01	0.351000E+01	0.805331E+01
β_3	0.263637E+02	0.198489E+02	0.587500E+01	0.390000E+01	0.254000E+01	0.827317E+01
β_4	0.137853E+02	0.809250E+01	0.525000E+01	0.303750E+01	0.214400E+01	0.793957E+01
β_5	0.491787E+01	0.609094E+01	0.452500E+01	0.224000E+01	0.154000E+01	0.757452E+01
β_6	0.447682E+01	0.601875E+01	0.423750E+01	0.165500E+01	0.112200E+01	0.396497E+01
β_7	0.304050E+01	0.593437E+01	0.218800E+01	0.116700E+01	0.800000E+00	0.285116E+01

*Read as 0.891397×10^5.

the vicinity of the equatorial plane, so that the infinitely thin current sheet is replaced by one having a finite thickness. The easiest way is to use $(z^2 + D^2)^{1/2}$ instead of $|z|$, as was done in T89. Another way is to replace $|z|$ by an interpolating function (either a parabola or a spline) for $|z| < D$, taking care to preserve the continuity of the first derivative at $z = \pm D$. In this case, the modification does not introduce any spurious electric current density outside the current layer (such currents, though very small, were present in the T87 and T89 models; they can be removed by using a similar method, as proposed by *Stern* [1990]). The last approach was used in the present work: instead of $|z|$, we substituted in (11)

$$\zeta = |z| \qquad\qquad |z| > D$$
$$\zeta = 0.5(z^2/D + D) \qquad |z| < D. \tag{13}$$

As mentioned above, one more desirable modification is the inclusion of hinging and warping of the current sheet in response to variations in the planetary dipole tilt angle Ψ. For relatively small tilt angles (as is the case in the Earth's magnetosphere) a realistic warped current sheet can be modeled through the replacement $z \to (z - z_s)$, where the function $z_s = z_s(x, y, \Psi)$ describes the shape and position of the current sheet and its dependence on the dipole tilt angle [e.g., *Tsyganenko*, 1989a]. Several studies have deduced the surface shape function z_s from observed neutral sheet crossings [*Russell and Brody*, 1967; *Fairfield*, 1980; *Gosling et al.*, 1986; *Dandouras*, 1988] or from model-fitting results [*Tsyganenko*, 1989a; *Stern*, 1990; *Peredo and Stern*, 1991; *Peredo et al.*, 1993].

To illustrate the technique introduced in the present study, we use the current sheet surface used by *Peredo et al.* [1993] in their derivation of a local tail model:

$$z_s(y, \Psi) = \left(R_H - G\,\frac{y^4}{y^4 + L_y^4}\right)\sin\Psi, \tag{14}$$

where $R_H = 7.02R_E$ gives the tail "hinging distance," while the amplitude $G = 34.03$ and the scale length $L_y = 19R_E$ control the spatial variation of the warping in the $y - z$ plane

(no x dependence was assumed in this particular example). Furthermore, as in the T89 model, the present treatment can also incorporate a spatially varying current sheet half-thickness $D(x, y)$. Summarizing the above two transformations, all occurrences of $|z|$ in (11) are replaced by

$$\zeta = |z - z_s(x, y, \Psi)| \qquad |z - z_s(x, y, \Psi)| > D(x, y) \tag{15a}$$

$$\zeta = 0.5\left[\frac{[z - z_s(x, y, \Psi)]^2}{D(x, y)} + D(x, y)\right] \tag{15b}$$
$$|z - z_s(x, y, \Psi)| < D(x, y).$$

After that, expressions for the components of the magnetic field $\mathbf{B} = \nabla \times \mathbf{A}$ and electric current density $\mathbf{j} = (1/\mu_0)\nabla \times \mathbf{B}$ can be found from (11) and (15) in a straightforward way. Figure 4 illustrates the north-south variation of the cross-tail
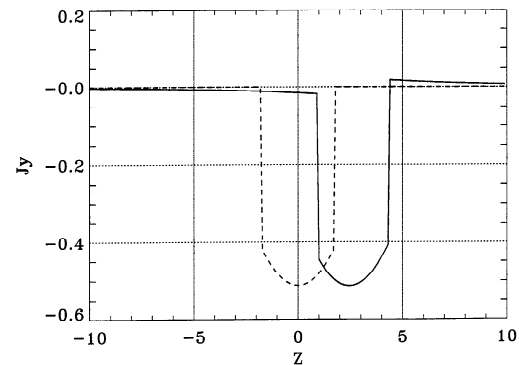
Figure 4. Plots of the distribution of j_y component of the electric current across the current sheet with a finite half-thickness $D = 1.72$ at $x = -10$ and $y = 10$. The dashed and solid curves are for untilted ($\Psi = 0$) and tilted ($\Psi = 35°$) dipoles, respectively, showing the effect of warping the current sheet as given by (14). In the tilted case, the current sheet is shifted in the positive z direction; a small artificial current density also emerges outside the current sheet, owing to the modification of the initially curl-free vector potential.

Equatorial Projection

Noon–Midnight Projection
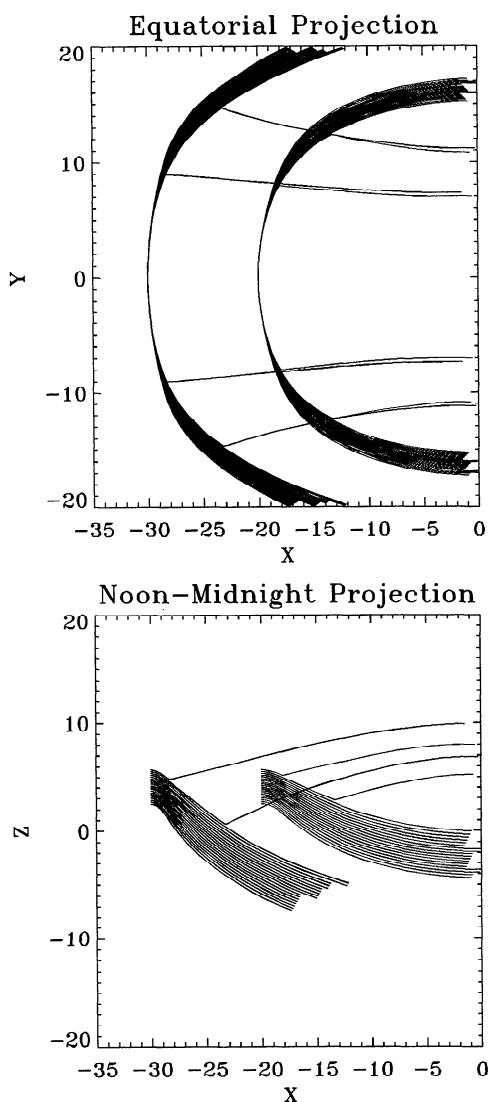
Figure 5. Two-dimensional projections of the electric current flow lines in the warped current disk ($\Psi = 30°$) crossing the midnight meridian plane at $x = -20$ and $x = -30$. A small amount of the current flows out of the sheet at its upper boundary, which is an artifact of the tilt-related deformation.

component of the current density for the slowest-mode solution with $L = 100$. The dashed curve in Figure 4 represents j_y for a configuration with zero dipole tilt angle, while the solid curve displays the corresponding density for a 35° tilt. In both cases a constant current sheet half-thickness $D = 1.72$ and the warped surface (14) have been used. The tilt-related deformation of the current sheet is illustrated in Figure 5, which shows two two-dimensional cuts of the electric current flow line structure for $\Psi = 35°$. The separation between neighboring current flow lines is such that a constant amount of current is contained between the lines. As seen in the plots, there is a small amount of in- and outflowing current at the sheet boundary; this effect, absent for $\Psi = 0$, is an artifact of the tilt-related modification of the vector potential and can also be noticed in the j_y profile shown in Figure 4 (solid curve).

The model current distributions described here are all ring-shaped, making them appropriate for modeling ring

currents, both that of the Earth and also much stronger ones like those of Jupiter and Saturn.

Such models are, however, also useful for modeling the field of the Earth's magnetotail current. The tail current sheet is observed to fit smoothly to the ring current [*Frank*, 1971; *Sugiura and Poros*, 1973], and its flow lines deduced from ratios B_y/B_x [*Tsyganenko et al.*, 1993] maintain gradually diminishing curvature throughout the near-Earth tail. As already noted, the T87 model is based on straight filaments and does a poor job of describing this curvature, which is why T89 was based on ring currents, as described in equations (2a)–(7).

While the use of ring currents in the tail allows curvature to be represented, a new problem arises: how to avoid an unphysical contribution from portions of the current flow outside the magnetopause. Ideally, the cross-tail current should be deflected upon reaching the magnetopause and should then continue along the surface.

In the T89 model, the vector potential A was modulated by a weight function $W(x, y)$, which indeed diverted the current but into a rather broad pattern. The effect of the closure current system was simulated by introducing a pair of additional current sheets shifted by 30–$40R_E$ in the z direction, each sheet carrying about half the current that was in the central sheet and flowing oppositely to the latter, that is, from dusk to dawn. However, this was just a "zero-order" solution, capable of taking into account only the gross effect of the return current system. A fundamentally different remedy which does have the desired effect is the confinement of the ring current inside a prescribed magnetopause surface by adding a magnetopause field represented by a scalar potential [*Voigt*, 1981; *Stern*, 1985; *Tsyganenko*, 1989b]; appropriate currents are then obtained by assuming $B = 0$ outside the boundary. The calculation of such shielding is beyond the scope of this study, but it should be noted that promising work in this direction was reported by *Sotirelis et al.* [1993] and will be presented in a later article.

6. Summary

We have presented a new analytical technique to describe the magnetic field from disklike electrical current sheets. The technique follows from an axially symmetric representation for the magnetic vector potential, leads to compact and flexible expressions for the magnetic field, and may be modified to represent nonaxisymmetric configurations. A sample configuration, corresponding to a warped current sheet like the one across the Earth's magnetotail, is used to illustrate the feasibility of the approach. Separate "modes" can readily be combined to simulate the tailward variation of the field and electric current in a realistic magnetotail; use of the vector potential facilitates inclusion of spatial variations in the current sheet thickness and/or tail warping effects due to tilt of the planetary dipole moment without violating the divergence-free condition. The proposed method can be used for quantitative modeling of the Earth's magnetotail and ring current field as well as those in the magnetospheres of Jupiter, Saturn, and other planets with similar magnetic field structures.

References

Behannon, K. W., Mapping of the Earth's bow shock and magnetic tail by Explorer 33, *J. Geophys. Res.*, *73*, 907, 1968.

Connerney, J. E. P., M. H. Acuña, and N. F. Ness, Modeling the Jovian current sheet and inner magnetosphere, *J. Geophys. Res.*, *86*, 8370, 1981.

Dandouras, J., On the average shape and position of the geomagnetic neutral sheet and its influence on plasma sheet statistical studies, *J. Geophys. Res.*, *93*, 7345, 1988.

Fairfield, D. H., A statistical determination of the shape and position of the geomagnetic neutral sheet, *J. Geophys. Res.*, *85*, 775, 1980.

Frank, L. A., Relationship of the plasma sheet, ring current, trapping boundary, and plasmapause near the magnetic equator and local midnight, *J. Geophys. Res.*, *76*, 2265, 1971.

Gosling, J. T., D. J. McComas, M. F. Thomsen, S. J. Bame, and C. T. Russell, The warped neutral sheet and plasma sheet in the near-Earth geomagnetic tail, *J. Geophys. Res.*, *91*, 7093, 1986.

Gradshteyn, I. S., and I. M. Ryzhik, *Table of Integrals, Series, and Products*, Academic, San Diego, Calif., 1980.

Lui, A. T. Y., R. W. McEntire, and S. M. Krimigis, Evolution of the ring current during two geomagnetic storms, *J. Geophys. Res.*, *92*, 7459, 1987.

Peredo, M., and D. P. Stern, On the position of the near-Earth neutral sheet: A comparison of magnetic model predictions with empirical formulas, *J. Geophys. Res.*, *96*, 19,521, 1991.

Peredo, M., D. P. Stern, and N. A. Tsyganenko, Are existing magnetospheric models excessively stretched?, *J. Geophys. Res.*, *98*, 15,343, 1993.

Russell, C. T., and K. I. Brody, Some remarks on the position and shape of the neutral sheet, *J. Geophys. Res.*, *72*, 6104, 1967.

Sergeev, V. A., and M. V. Malkov, Diagnostics of the magnetic configuration of the plasma layer from measurements of energetic electrons above the ionosphere, *Geomagn. Aeron., Engl. Transl.*, *28*, 549, 1988.

Sotirelis, T., D. P. Stern, and N. A. Tsyganenko, A method for modeling the magnetopause field in the tail (abstract), *Eos Trans. AGU*, *74*(16), Spring Meeting, suppl., 273, 1993.

Stern, D. P., Parabolic harmonics in magnetospheric modeling: The main dipole and the ring current, *J. Geophys. Res.*, *90*, 10,851, 1985.

Stern, D. P., A model of the magnetospheric tail with current-free lobes, *Planet. Space Sci.*, *38*, 255, 1990.

Stern, D. P., and N. A. Tsyganenko, Uses and limitations of the Tsyganenko magnetic field models, *Eos Trans. AGU*, *73*(46), 489, 1992.

Sugiura, M., and D. J. Poros, A magnetospheric field model incorporating the OGO 3 and 5 magnetic field observations, *Planet. Space Sci.*, *21*, 1763, 1973.

Tsyganenko, N. A., Global quantitative models of the geomagnetic field in the cislunar magnetosphere for different disturbance levels, *Planet. Space Sci.*, *35*, 1347, 1987.

Tsyganenko, N. A., A model of the magnetospheric magnetic field with a warped tail current sheet, *Planet. Space Sci.*, *37*, 5, 1989a.

Tsyganenko, N. A., A solution of the Chapman-Ferraro problem for an ellipsoidal magnetopause, *Planet. Space Sci.*, *37*, 1037, 1989b.

Tsyganenko, N. A., Quantitative models of the magnetospheric magnetic field: Methods and results, *Space Sci. Rev.*, *54*, 75, 1990.

Tsyganenko, N. A., and A. V. Usmanov, Determination of the magnetospheric current system parameters and development of experimental geomagnetic field models based on data from IMP and HEOS satellites, *Planet. Space Sci.*, *30*, 985, 1982.

Tsyganenko, N. A., D. P. Stern, and Z. Kaymaz, Birkeland currents in the plasma sheet, *J. Geophys. Res.*, *98*, 19,455, 1993.

Voigt, G.-H., A mathematical magnetospheric field model with independent physical parameters, *Planet. Space Sci.*, *29*, 1, 1981.

M. Peredo, Laboratory for Extraterrestrial Physics, Hughes STX Corporation at NASA Goddard Space Flight Center, Greenbelt, MD 20771.

N. A. Tsyganenko, Laboratory for Extraterrestrial Physics, NASA Goddard Space Flight Center, Greenbelt, MD 20771.